Curvature-Directed Crystallization of Poly(vinylidene difluoride) in Nanotube Walls

Martin Steinhart,[*,†,‡] **Stephan Senz,**[‡] **Ralf B. Wehrspohn,**[‡] **Ulrich Gösele,**[‡] **and Joachim H. Wendorff**[†]

Institute of Physical Chemistry and Center of Materials Science, Philipps-University, Hans-Meerwein-Strasse, 35032 Marburg, Germany, and Max-Planck-Institute of Microstructure Physics, Weinberg 2, 06120 Halle, Germany

Received December 24, 2002; Revised Manuscript Received March 21, 2003

ABSTRACT: Poly(vinylidene difluoride) (PVDF) nanotubes were prepared by wetting of ordered porous templates. We processed either PVDF melts or solutions. The properties of the nanotubes depend strongly on the preparation method. Solution-wetting provides nanotube walls with poor crystallinity. In contrast, nanotube walls obtained by melt-wetting exhibit a pronounced crystallinity indicating the formation of a brushlike wetting layer. The crystallites grow preferentially in the direction of minimal curvature, which corresponds to the long axis of the nanotube. The crystal facets with the highest growth rate are oriented perpendicularly to this axis. For nanotubes consisting of α-PVDF, X-ray diffraction revealed that the *b*-axis of the unit cell is oriented parallel to the long axis of the nanotube.

1. Introduction

Tubular nanostructures with dimensions in the 100 nm range have attracted increasing interest during the past decade.[1−14] Various preparation processes have been reported based on either self-assembly[1−7] or the use of templates.[8−14] The synthesis of nanotubes within the nanoscaled pores of a matrix provides nanotubes consisting of numerous wall materials ranging from polymers to metals.[8−10] However, nanostructuring of functional polymers and the functionalization of nanotubes are still challenges in materials science. Wetting of porous templates by polymer melts or solutions has turned out to be a versatile technique to form nanotubes from a broad range of material systems, including high-performance polymers such as poly(tetrafluoroethylene) or multicomponent mixtures.[15] It is based on the fact that any liquid containing polymers wets the walls of nanoporous templates avidly if the walls exhibit a high surface energy. A mesoscopic layer of the liquid will thus cover the pore walls completely after a short time. The process can be frozen conveniently at this stage to preserve tubular structures within the template pores. Optionally, the template can be removed selectively to prepare either powders or arrays of free-standing nanotubes. They have wall thicknesses of the order of 10 nm, whereas their outer diameter ranges from a few tens of nanometers up to a few microns.

The properties of the nanotubes will depend largely on the morphology of their walls. Decomposition into coexisting phases was successfully employed to generate a fine structure within electrospun nanofibers.[16,17] Therefore, it should be a promising route toward a specific wall morphology and thus toward functionalized nanotubes to couple the wetting procedure with phase transitions within the nanotube walls. Indeed, the phase morphology within the walls of palladium/polylactide composite nanotubes obtained by wetting of porous alumina could be tailored by controlled ripening.[18]

However, one of the most important processes to generate an internal fine structure within polymeric specimens is crystallization. Partially crystalline polymers are both ideal one-component model systems and of considerable interest for various applications, since the mechanical, electronical, and optical properties of such materials depend largely on the properties of the crystalline domains. If the polymeric melt is cooled to a temperature well below the melting point after the wetting of the walls of the template pores, crystallization may occur. The geometry of the nanotube walls imposes constraints, since their thickness and their perimeter are finite. The system is infinite only in the direction of the tube axis. Moreover, the curvature of the pore wall should affect the crystallization. It is crucial to gain an understanding of crystallization processes within the nanotube walls in order to control the generation of the wall morphologies.

We investigated these phenomena for the particular case of poly(vinylidene difluoride) (PVDF) nanotubes. We selected this polymer owing to the piezoelectric properties of some of its crystal modifications and the considerable potential of PVDF nanotubes for applications in the field of ultrafiltration.[19] In the following, we will particularly evaluate whether crystallization occurs within the nanotube walls and whether the nanotube walls exihibit directional crystal growth due to their confined geometry and curvature. If this is the case, it will have implications for the use of nanotubes as building blocks for miniaturized devices, since an anisotropic structure of the nanotube walls is favorable or even a prerequisite for many applications.

2. Experimental Section

Templates. We used both ordered porous alumina[20] and ordered macroporous silicon[21] with pore diameters D_p ranging from 400 nm to 1 μm and pore depths T_p ranging from 50 to 100 μm as templates. Their preparation is described elsewhere.[22,23] The alumina templates were cleaned by immersing them into solvents of different polarity (deionized water, ethanol, acetone, chloroform, and hexane) and applying ultrasound. Silicon templates were cleaned by immersing them into nitric acid for 24 h and rinsing the templates with deionized water and acetone several times.

[†] Philipps-University.
[‡] Max-Planck-Institute of Microstructure Physics.
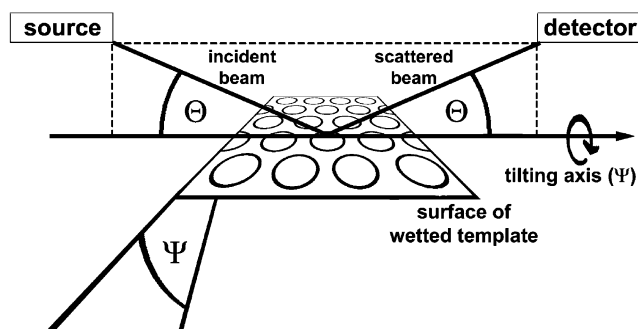[*] Corresponding author: e-mail steinhar@mpi-halle.de.

Table 1. Preparation Details of the Samples 58, 105, 108, 311, and 315

sample	material	porous template
58	Solvay 1008, M_w = 100 000 g/mol, M_n = 38 000 g/mol	ordered macroporous silicon, D_p = 400 nm, T_p = 50 μm
105	Aldrich, M_w = 180 000 g/mol, M_n = 71 000 g/mol	ordered macroporous silicon, D_p = 1 μm, T_p = 100 μm
311	Aldrich, M_w = 180 000 g/mol, M_n = 71 000 g/mol	ordered alumina, D_p = 400 nm, T_p = 50 μm
315	Aldrich, M_w = 180 000 g/mol, M_n = 71 000 g/mol	ordered alumina, D_p = 400 nm, T_p = 50 μm
108	Aldrich, M_w = 180 000 g/mol, M_n = 71 000 g/mol	none, molten pellets on an aluminum substrate
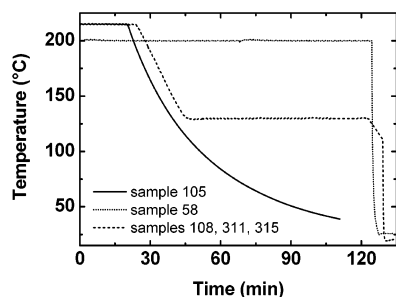
Figure 1. Temperature profiles applied to the samples 58, 105, 108, 311, and 315 during their preparation.

Figure 2. Schematic depiction of the setup used for the X-ray diffraction experiments. For the $\Theta/2\Theta$ scans the samples were placed in the device in such a way that the surface of the wetted template was oriented perpendicular to the plane of incident and scattered X-ray beam. To perform the Ψ scans, the setup was adjusted to selected 2Θ angles. Then, the samples were tilted by an angle Ψ around an axis defined by the intersection of the template surface and the plane of the incident and the scattered X-ray beam. The scattering intensity was measured as a function of the tilting angle Ψ.

Preparation of PVDF Nanotubes. The apparatus used for the preparation procedure consisted of an oven with a cylindrical inner space that was operated by an Eurotherm V2604 temperature controller. The temperature profiles of all experiments were recorded. The oven was connected both to a vacuum pump and an argon supply. This setup allowed to protect the samples from moisture and oxygen when the coverage of the oven was removed. To prepare PVDF nanotubes by melt-wetting, the templates were placed in the oven in an argon atmosphere. Then, we placed PVDF pellets with tweezers on the template at temperatures of 200 or 215 °C, well above its melting point of 178 °C. To prepare PVDF nanotubes by solution-wetting, we used solutions containing 10 wt % PVDF in dimethylformamide (DMF). They were dropped on the templates from a syringe under ambient conditions. After the evaporation of the solvent, we removed the residual PVDF on the top of the template and placed the wetted templates in the preheated oven. Subsequently, the samples were annealed under vacuum. To control the crystallinity, the temperature profile and the cooling rates were chosen properly. After cooling the oven down to room temperature, the samples were removed. Table 1 gives an overview over the samples and the templates used. The temperature profile of each sample is shown in Figure 1.

Characterization of PVDF Nanotubes by Scanning Electron Microscopy (SEM). SEM micrographs were recorded with a JEOL JSM 6300 F scanning electron microscope. We prepared the samples either as an array or as a powder. To remove the template material selectively, it was etched with 40 wt % aqueous potassium hydroxide (KOH) at room temperature in the case of porous alumina and at 60 °C in the case of macroporous silicon. To prepare arrays, we glued the wetted templates on conducting copper substrates prior to the removal of the matrix material using a conductive glue. The arrays could be handled with tweezers and thus be washed by immersing them into liquids. To remove residual KOH, the samples were washed several times with diluted hydrochloric acid, deionized water, and ethanol. To obtain the PVDF nanotubes as a powder, we removed the residual PVDF on the top of the template prior to etching. We moved the wetted templates into cuvettes filled with aqueous KOH. The resulting suspension within the cuvettes was centrifuged after the complete decomposition of the matrix material. Then, the lye was removed with a syringe. The powder samples were washed by adding deionized water or ethanol. After centrifuging, the liquids were separated from the precipitation consisting of the PVDF nanotubes. Finally, they were prepared as ethanolic suspensions that were dropped on silicon wafer. Prior to the SEM investigations, both the nanotube powders and arrays were covered by gold.

Characterization of PVDF Nanotubes by Optical Microscopy. A silicon template with a pore diameter D_p = 1 μm was wetted with a PVDF melt. The template was etched, and the lye was removed subsequently. Then, the nanotubes were washed as described above. A suspension of the tubes in ethanol was dropped on a glass slide. Then we investigated the sample with an oil immersion microscope Leica DMR in the transmitted light modus and between crossed polarizers. The images were recorded with a CCD camera.

Characterization of PVDF Nanotubes by X-ray Diffraction (XRD). XRD measurements were performed using a Philips X'pert MRD diffractometer with cradle and secondary monochromator for Cu Kα radiation. We investigated both melt-wetted and solution-wetted alumina templates (D_p = 400 nm) by XRD. After the wetting procedure, the residual polymer on the top side of the templates was carefully removed with a scalpel. SEM investigations revealed that the pore openings were uncovered. $\Theta/2\Theta$ scans were carried out in the reflection mode with an 2Θ increment of 0.05° and an integration time of 20 s. The samples were placed in the diffractometer in such a way that the template surface with the pore openings was arranged perpendicular with respect to the plane defined by the incident and the scattered X-ray beams (Figure 2, Ψ = 0°). The nanotubes were well-aligned within the templates during the measurements.

To investigate the textures of the samples, we performed in addition to the $\Theta/2\Theta$ scans so-called Ψ-scans. The settings of Θ (incident beam) and 2Θ (detector) were fixed to specific values. The sample was tilted by an angle Ψ around the axis defined by the intersection of the plane of the incident and the scattered X-ray beams with the template surface. The setup is displayed schematically in Figure 2. Ψ equals zero if the two planes are oriented perpendicularly. The scattering intensity is measured as a function of the tilting angle Ψ. This method allows to record a fiber diffractogram in reflection mode. The Ψ-scans were performed with an increment of 1° and an integration time of 10 s.

3. Results and Discussion

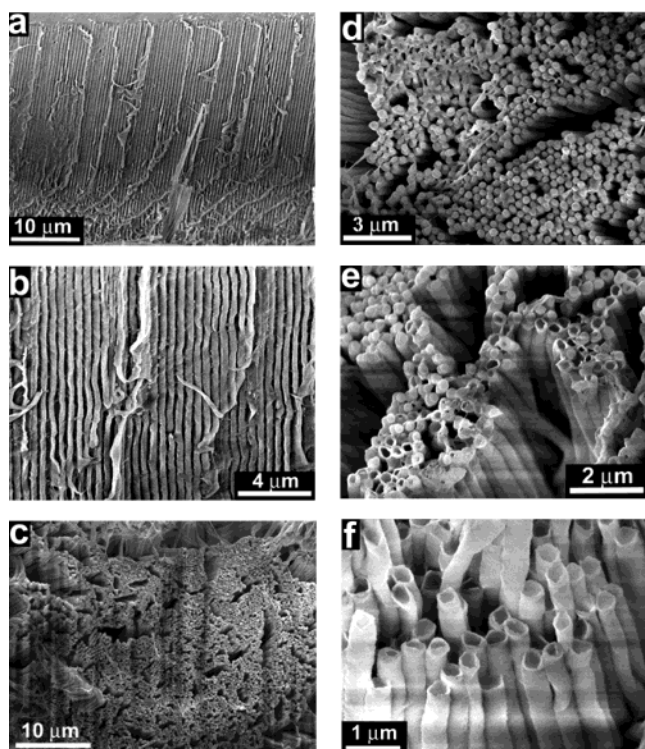Wetting of porous templates consisting of both alumina and silicon with PVDF melts yielded PVDF

Figure 3. Scanning electron micrographs of sample 58 prepared by wetting of macroporous silicon with a PVDF melt. (a, b) Cross sections of the macroporous silicon template wetted with PVDF. Well-aligned PVDF nanotubes are observable. (c, d) Top view on an array of PVDF nanotubes after the selective removal of the template material. (e, f) PVDF nanotubes whose caps (replicas of the pore bottoms) broke off, so that their hollow character becomes detectable.

nanotubes. The polymer was allowed to wet ordered macroporous silicon (D_p = 400 nm; T_p = 50 μm, sample 58) for 2 h at 200 °C prior to quenching to room temperature. A cross section of the silicon template after the wetting process is shown in Figure 3a,b. The pore walls were covered with a mesoscopic PVDF film completely over their entire depth, and well-aligned nanotubes with a length corresponding to the pore depth are observable. Even after the selective removal of the template, the hexagonal arrangement of the template pores was partially preserved within the PVDF nanotube array shown in Figure 3c,d. Figure 3e,f shows some open-ended nanotubes, which have lost their caps. The wall thickness was estimated to be 30 nm.

PVDF nanotubes were also obtained by wetting of templates with solutions of 10 wt % PVDF in DMF (sample 311). After wetting of an alumina template (D_p = 400 nm; T_p = 50 μm), the residual PVDF on the top of the template was removed mechanically. Then, the sample was annealed for 30 min at 215 °C, cooled to 130 °C within 25 min, and annealed for 70 min at this temperature prior to a quench to room temperature (Figure 1). The pore openings of a wetted template after the annealing procedure are depicted in Figure 4a. The pore opening in the center is partially covered by a part of the nanotube wall. Finally, the template was removed selectively. The walls of the nanotubes exhibit voids and defects (Figure 4b). Openings of the nanotubes are shown in Figure 4c,d at higher magnifications.

The question arises whether crystallization occurs within the nanotube walls and, if so, whether the wall morphology exhibits a well-defined orientation of the
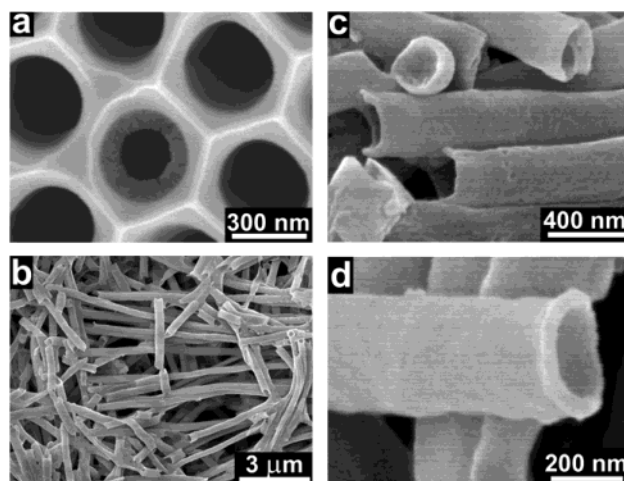

Figure 4. Scanning electron micrographs of sample 311 prepared by wetting of porous alumina with a solution of PVDF in DMF. (a) Top of a porous alumina template after the wetting procedure. The pore opening in the center is partially covered by a nanotube wall. (b) Nanotubes after the selective removal of the template material, prepared as powder. (c, d) Detailed view of the openings of the nanotubes.

crystal axes. The geometry of the nanotube walls imposes geometrical constraints that are different from those occurring in thin films on smooth substrates. The wall thickness, but also the perimeter of the nanotubes, are finite. Moreover, the curvature of the nanotube walls may have an impact on the structure formation. PVDF nanotubes obtained by melt-wetting of an ordered silicon template with D_p = 1 μm (sample 105) were investigated by optical microscopy. The sample was annealed for 20 min at 215 °C and subsequently cooled to room temperature slowly by switching off the heating (Figure 1). Figure 5a depicts a transmitted light micrograph of an individual PVDF nanotube after removing the template. Apparently, there is a continuous hollow space inside. Between crossed polarizers, it exihibits birefringence (Figure 5b). This is a signature of cystallinity.

To gain further information on the internal morphology, we performed XRD experiments on wetted templates. We used alumina templates for this purpose since there are no disturbing reflections originating from the template material at 2Θ values smaller than 40°. We investigated three samples. The first one was a film of molten PVDF pellets (sample 108), and the second was an alumina template (D_p = 400 nm, T_p = 50 μm) wetted with a PVDF melt (sample 315). The samples were prepared by placing PVDF pellets on an aluminum substrate (108) or on the template (315) in an oven with a temperature of 215 °C. The third sample was a part of the solution-wetted sample 311. It was obtained by wetting the same alumina template as in the case of sample 315 at ambient conditions. As described above, the residual PVDF film was removed from the top of the template. Then, it was placed in the oven that was heated to 215 °C.

All samples were annealed at 215 °C well above the melting point of PVDF for 30 min and cooled to 130 °C. Since the presence of several modifications would complicate the detection of a texture, the samples were annealed for 70 min at this relatively low temperature prior to quenching to room temperature (Figure 1). Under these conditions, PVDF should crystallize in the α-form exclusively, whereas crystallization at higher
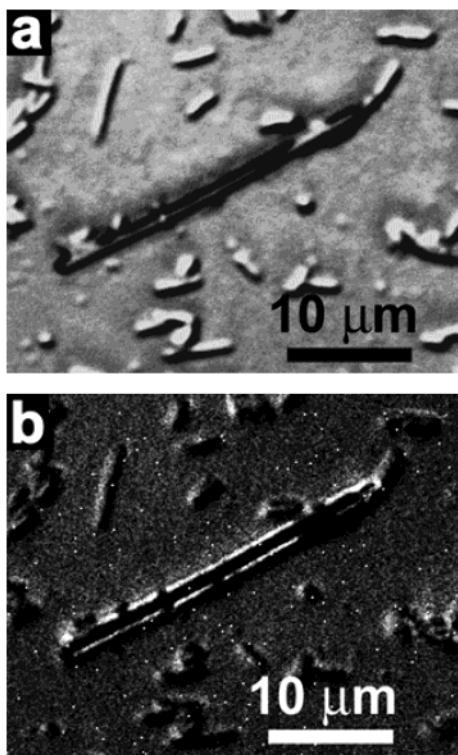
Figure 5. Optical micrographs of an individual PVDF nanotube (sample 105) after the selective removal of the template obtained by using an oil immersion objective: (a) transmitted light micrograph and (b) the same PVDF nanotube as in (a) between crossed polarizers.

Table 2. 2Θ Values of the Reflections of α-PVDF According to Ref 25 and 2Θ Values Obtained for Samples 108 and 315 (Integration Time for Θ/2Θ Scans 20 s, Increment 0.05°)[a]

reflection	2θ (deg) according to ref 25	108 2Θ (deg)	315 2Θ (deg)
(100)	17.868	17.7	
(020)	18.392	18.4	18.3
(110)	20.119	20.0	19.9
(120)	25.751	25.8	
(021)	26.706	26.7	
(111)	27.945	27.9	
(121)	32.319	32.2	
(130)	33.193	33.2	
(200)	36.190	35.9	
(040)	37.280	37.1	37.0
(131)	38.625	38.6	

[a] In the case of sample 315, the reflection at 2Θ = 19.9° was very weak.

temperatures may yields mixtures of different modifications including the polar β-modification.[24]

Sample 108 represents bulk PVDF; i.e., this sample should not exhibit a texture. In the case of the samples 311 and 315, the PVDF nanotubes are perfectly aligned inside the template. If they show a texture, it should thus be detectable.

The reflections occurring in the diffractograms obtained by the Θ/2Θ scans of the samples 108 and 315 as well as the 2Θ values and the corresponding (*hkl*) indices from ref 25 are listed in Table 2. The respective diffractograms as well as the one of sample 311 are shown in Figure 6a. As expected, sample 108 consisted of α-PVDF (also referred to as "form II"), and no manifestations of anisotropy were detected. Only one pronounced reflection at 18.3° occurred in the case of sample 315. The comparison with the diffractogram of
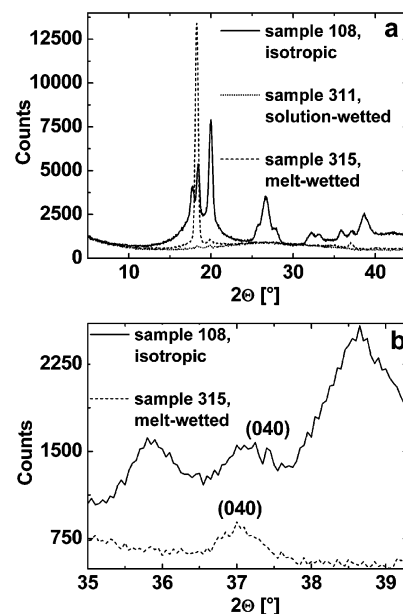

Figure 6. Θ/2Θ scans of samples 108, 311, and 315. The PVDF nanotubes were well-aligned within the alumina templates (D_p = 400 nm) during the measurements in the reflection mode. The wetted templates were placed on the device in such a way that the template surface with the pore openings was oriented perpendicular to the plane defined by the incident and scattered X-ray beam. The increment was 0.05° and an integration time 20 s for each step. (a) Overview. (b) 2Θ range around the (040) reflection of samples 108 and 315.

sample 108 and the data from ref 25 reveals that this reflection corresponds to the (020) reflection of α-PVDF. The most intensive (110) reflection at 19.9° of the isotropic sample 108 is very weak in the diffractogram of sample 315, just distinguishable from the noise. Both samples 108 and 315 exhibit the (040) reflection at 37.1° and 37.0°, respectively (Figure 6b). Other reflections expected for α-PVDF did not occur at all during the Θ/2Θ measurement of sample 315. The diffraction pattern of sample 311 consists of only two very weak reflections for 2Θ values of 18.3° and 19.9°. Hence, the PVDF within the nanotube walls of sample 315 is well-crystallized and exhibits a pronounced texture. Only very weak crystalline reflections were detected in the case of sample 311, although it was treated thermally in the same manner as the melt-wetted sample 315. Sample 311 has thus only a very poor degree of crystallinity, if any.

It is a striking result that wetting of the porous templates by PVDF melts yields nanotubes with a pronounced crystallinity whereas solution-wetting results in the formation of largely amorphous nanotubes. Currently, we can only speculate that wetting from solutions yields wetting layers with a structure different from those obtained by melt-wetting. Polymers may adsorb in the form of brushes corresponding to a large number of adsorbed chains per area (Figure 7a) or in a mushroomlike form corresponding to a lower surface coverage (Figure 7b).[26] We assume that polymeric brushes are obtained by melt-wetting whereas solution-wetting results in the formation of nanotube walls composed rather of polymer chains with a mushroom-type conformation. It is obvious that brushlike layers should crystallize avidly whereas the polymer chains within mushroom-type layers cannot arrange themselves in a manner favorable for crystallization. If these assump-
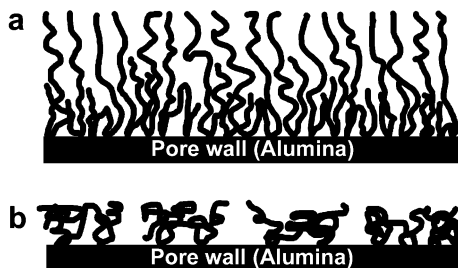
Figure 7. Different adsorption regimes for polymers on surfaces: (a) brushlike adsorption layer, (b) mushroomlike adsorption layer.

tions are true, the properties of nanotube walls will depend largely on whether the wetting procedure is performed using a solution in a good, a poor, a Θ solvent, or a melt without additional components.

To investigate the anisotropic X-ray pattern of sample 315 in more detail, we performed Ψ scans for several 2Θ angles as described in section 2 (Figure 2). For a 2Θ value of 18.3° corresponding to the (020) reflection a sharp intensity maximum occurred at Ψ = 0°. The (020) and consequently the (040) lattice planes must be arranged parallel to the template surface and thus perpendicular to the long axes of the template pores and the PVDF nanotubes, respectively. Therefore, the *b*-axis of the unit cell of α-PVDF is oriented parallel to the long axis of the nanotubes. Most of the crystallites are oriented such that they contribute to the scattering intensity only if Ψ equals zero. If a cross section of a PVDF nanotube perpendicular to the long axis is considered, the orientation of the {0*k*0} lattice planes remains invariant for any position within the wall. In contrast, such lattice planes whose *h*- and *l*-indices are not equal to zero alter their orientation relative to the orientation at a reference point on the nanotube wall such that the *a*-axis is parallel and the *c*-axis perpendicular to the tangent on the nanotube wall at the current position. We measured Ψ scans for several further 2Θ values corresponding to reflections having a relatively large intensity in the case of the isotropic sample 108. Theoretically, the interplanar angles of the (020) and the (110), the (120), and the (021) lattice planes equal 62.8°, 44.2°, and 46.2°, respectively. These interplanar angles correspond to the tilting angles Ψ at which scattering intensity originating from crystallites fulfilling the Bragg condition should be detectable for the respective adjusted 2Θ values of 19.9°, 25.6°, and 26.5°. The results are displayed in Figure 8a,b.

The Ψ scans for the 2Θ values of 19.9°, 25.6°, and 26.5° show actually maxima at Ψ = 56°, Ψ = 40°, and Ψ = 43°, respectively, but there is a significant shift to smaller angles compared to the theoretical values. For geometrical reasons, the sensitivity of the Ψ scans decreases with increasing Ψ values. This distorts the peaks and shifts their maxima to lower values. For the 2Θ values of 17.6° corresponding to the (100) reflection and 27.9° corresponding to the (111) reflection no maxima were detected. In the case of the (100) reflection a maximum should occur at Ψ = 90°. However, since the sensitivity of this method decreases with increasing Ψ, this maximum is not detectable. In the case of the (111) reflection, we assume that the intensity of the reflection is simply too low to obtain a distinctive maximum at the expected Ψ value of 70.7°. The PVDF nanotubes obviously exhibit a pronounced texture that resembles the one found by Lovinger and Wang for directionally solidified PVDF films.[27]
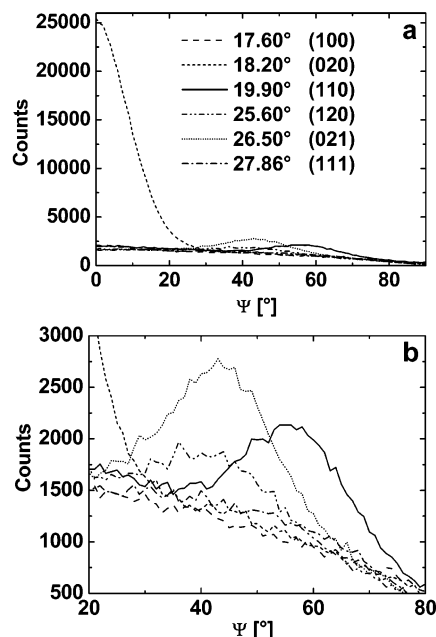

Figure 8. Ψ scans of sample 315 for several 2Θ values. The wetted templates were measured in reflection mode as described in section 2 and displayed in Figure 2. (a) Entire Ψ range; (b) magnification of a part of (a).
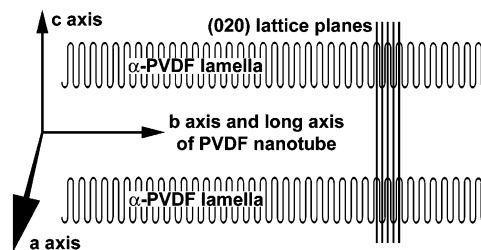

Figure 9. Schematic structure model of the wall of a PVDF nanotube. The crystallites are preferentially oriented such that the crystallographic *b*-axis of α-PVDF is parallel to the long axis of the template pore and the long axis of the PVDF nanotube, respectively. The (020) lattice planes (as well as the (040) lattice planes) are parallel to the template surface, whereas the polymer chains were oriented perpendicularly to the pore walls and the long axis.

If these results are compared with the crystal structure reported by Hasegawa et al.,[28] we arrive at the structure model of the nanotube wall shown in Figure 9: the PVDF chains within the crystallites are oriented perpendicularly to the long axis of the nanotubes and the pore walls of the template. The crystallites thus adapt the curvature imposed by the pore geometry. It is well-known that crystallites of α-PVDF grow preferentially in the direction of the *b*-axis; i.e., the (020) facets have the highest growth rate.[24,27] Within the walls of the PVDF nanotubes they are oriented perpendicularly to the direction of the lowest curvature. The only growth direction showing no curvature is the one parallel to the long axis of the nanotubes. The crystal growth occurs consequently in such a way that the crystallographic *b* axis as the major growth axis is oriented parallel to the long axis of the nanotubes. This is schematically sketched in Figure 10.

A texture can be induced by geometric constraints. In systems that are infinite only in one direction, the growth axis aligns with the long axis of the confined space.[29] However, we suggest that the wall curvature strongly influences the crystallization. The magnitude of the curvature is such that it should affect structure

Figure 10. Orientation of the crystallographic *b*-axis of α-PVDF with respect to the curvature of the nanotube wall. The crystal growth occurs preferentially in the direction of the *b*-axis, the only one where the curvature equals zero.

formation processes characterized by mesoscopic correlation lengths which are typical for polymers. In the case of nanotubes with a diameter of 400 nm, the perimeter equals 1256 nm. If a lamella grows 50 nm in the circumference direction of the wall, it will be tilted nearly 15° compared to its original orientation at the starting point. Preliminary investigations revealed that the preferential orientation of the crystallites depends to a great extend on the magnitude of the wall curvature. The pronounced texture found for sample 315 should thus be the result of a curvature-directed crystallization. If the processing conditions are optimized, nanotubes containing directionally grown crystallites of polar crystal modifications may be accessible.

4. Conclusions

Wetting of porous templates is a versatile method, which allows to form high-performance polymers as well as multicomponent systems into nanotubes. Phase transitions within their walls, in particular crystallization, affect their properties but allow also to tailor their morphologies. We investigated nanotubes consisting of PVDF as a partially crystalline model polymer. If they are obtained by wetting of porous templates with PVDF solutions in dimethylformamide, they are largely amorphous. In contrast, nanotubes that were prepared by wetting with PVDF melts exhibited a pronounced crystallinity. Moreover, the crystallites were strongly oriented such that the crystal facets exhibiting the highest growth rate are perpendicular to the direction of the lowest curvature. Directed crystal growth occurs thus in the direction of the long axis of the nanotubes. Consequently, this phenomenon can be referred to as curvature-directed crystallization, and it may be of considerable interest for designing nanotubes as building blocks for nanophotonics and nanoelectronics.

References and Notes

(1) Whitesides, G. M.; Mathias, J. P.; Seto, C. T. *Science* **1991**, *254*, 1312.
(2) Ozin, G. A. *Adv. Mater.* **1992**, *4*, 612.
(3) Schnur, J. M. *Science* **1993**, *262*, 1669.
(4) Ghadiri, M.; Granja, J. R.; Buehler, L. K. *Nature (London)* **1994**, *369*, 301.
(5) Edelmann, F. T. *Angew. Chem.* **1999**, *111*, 1473; *Angew. Chem., Int. Ed.* **1999**, *38*, 1381.
(6) Iijima, S. *Nature (London)* **1991**, *354*, 56.
(7) Schmidt, O. G.; Eberl, K. *Nature (London)* **2001**, *410*, 168.
(8) Martin, C. R. *Science* **1994**, *266*, 1961.
(9) Martin, C. R. *Acc. Chem. Res.* **1995**, *28*, 61.
(10) Hulteen, J. C.; Martin, C. R. *J. Mater. Chem.* **1997**, *7*, 1075.
(11) Evans, E.; Brownman, H.; Leung, A.; Needham, D.; Tirrell, D. *Science* **1996**, *273*, 933.
(12) Bognitzki, M.; Hou, H.; Ishaque, M.; Frese, T.; Hellwig, M.; Schwarte, C.; Schaper, A.; Wendorff, J. H.; Greiner, A. *Adv. Mater.* **2000**, *12*, 637.
(13) Caruso, R. A.; Schattka, J. H.; Greiner, A. *Adv. Mater.* **2001**, *13*, 1577.
(14) Mayya, K. S.; Gittins, D. I.; Dibaj, A. M.; Caruso, F. *Nano Lett.* **2001**, *1*, 727.
(15) Steinhart, M.; Wendorff, J. H.; Greiner, A.; Wehrspohn, R. B.; Nielsch, K.; Schilling, J.; Choi, J.; Gösele, U. *Science* **2002**, *296*, 1997.
(16) Bognitzki, M.; Czado, W.; Frese, T.; Schaper, A.; Hellwig, M.; Steinhart, M.; Greiner, A.; Wendorff, J. H. *Adv. Mater.* **2001**, *13*, 70.
(17) Bognitzki, M.; Frese, T.; Steinhart, M.; Greiner, A.; Wendorff, J. H.; Schaper, A.; Hellwig, M. *Polym. Eng. Sci.* **2001**, *41*, 982.
(18) Steinhart, M.; Jia, Z.; Schaper, A.; Wehrspohn, R. B.; Gösele, U.; Wendorff, J. H., submitted to *Adv. Mater.*
(19) *Ullmann's Encyclopedia of Industrial Chemistry*, 6th ed.; Electronic release; Wiley-VCH: Weinheim, 2002.
(20) Masuda, H.; Fukuda, K. *Science* **1995**, *268*, 1466.
(21) Lehmann, V. *J. Electrochem. Soc.* **1993**, *140*, 2836.
(22) Nielsch, K.; Choi, J.; Schwirn, K.; Wehrspohn, R. B.; Gösele, U. *Nano Lett.* **2002**, *2*, 677.
(23) Birner, A.; Wehrspohn, R. B.; Gösele, U.; Busch, K. *Adv. Mater.* **2001**, *13*, 377.
(24) Lovinger, A. J. *J. Polym. Sci., Part B* **1980**, *18*, 739.
(25) JCPDS database, entry no. 42-1650.
(26) Israelachvili, J. *Intermolecular and Surface Forces*, 2nd ed.; Academic Press: London, 1991; pp 289−293.
(27) Lovinger, A. J.; Wang, T. T. *Polymer* **1979**, *20*, 725.
(28) Hasegawa, R.; Takahashi, Y.; Chatani, Y.; Tadokoro, H. *Polym. J.* **1972**, *3*, 600.
(29) Schultz, J. M. *J. Polym. Sci., Part B* **1992**, *30*, 785.